Experiments on Ion Cyclotron Heating of Plasma in the Heliotron-B Device

By

Shigenori HAYASHI* and Akihiro MOHRI*

(Received May 31, 1956)

The Heliotron magnetic field for plasma confining has many magnetic slopes suitable to cause a phase mixing of ion cyclotron waves propagating along the magnetic lines of force. Experiments on ion cyclotron heating with this mechanism were carried out by using a plasma generator "Heliotron-B". A *rf* coil of Picket Fence type fed *rf* power into plasma and excited the ion cyclotron waves of 12 cm axial wave length.

Rf power absorption curves as a function of *rf* frequency, obtained by using a low power oscillator, showed there are two kinds of *rf* loading peaks of plasma; one is due to the excitation of the ion cyclotron waves and another due to the cyclotron resonance of individual ions. The exciting efficiency of the ion cyclotron waves was above 75%. Doppler shifts of particle cyclotron reasonance from the cyclotron frequency were also observed under the Joule heating. This fact suggests that ion beams are flowing in plasma under the Joule heating.

The plasma generated by the Joule heating was supplied with *rf* power of 100 kW, and ion cyclotron waves were excited and damped in the Heliotron field. As a results, ion temperature could be raised up to 4×10^5 °K. Electron temperature was insensible to this heating.

1. Introduction

Ion cyclotron heating of plasma is thought to be a hopeful method to heat plasma up to extremely high temperature necessary for thermonuclear fusion. Therefore, this heating method has been examined at many places. Attainable electron temperature by Joule heating is generally upper bounded within the order of 10^6 in degrees Kelvin. Ion temperature can not rise to that value by this method, since the equipartition time of temperature between ions and electrons is very long, especially for tenuous plasma. It will be one of the most suitable processes that gas is first brought to a fully ionized plasma at relatively high electron temperature by Joule heating and then ion cyclotron heating raise its ion temperature.

* Department of Electrical Engineering, II

Ion cyclotron waves with an axisymmetric mode were first found by Stix (1958)[1]. He and his collaborators gave experimental evidence for the existence of these waves by using Stellarators B-65 and B-66[2,3]. The damping of ion cyclotron waves was analyzed by Stix on the basis of linearized theory[4]. Its nonlinear treatment was done by Hasegawa and Birsall[5]. They demonstrated that ion cyclotron waves are easily subjected to a phase mixing where the wave frequency is near the cyclotron frequency. This damping is called "cyclotron damping" and the damping region is also called "Magnetic beach". Bakaev, Zaleskii, Mazarov, Ukrainskii and Torok (1962)[6] observed the generation and absorption of ion cyclotron waves in a moving plasmoid and a Doppler effect occurring from the plasmoid velocity. These experiments above referred were done by using induced *rf* field of Picket Fence configuration. Machines, that have a torus shape and the magnetic beach region, are only Stellarator C[7] and the Heliotron-B.

The Heliotron-B has a so-called Heliotron magnetic field corrugating along the torus axis and its wavy form can be adjusted by changing magnetic coil connections. Thus many different undulating magnetic fields can be generated. These field, consequently, have many magnetic slopes appropriate for the cyclotron damping of ion cyclotron waves. If ion cyclotron waves excited in a *rf* coil region propagate into the Heliotron magnetic field, thermalization of the waves and heating of ions will be expected. Experiments described herein concern single-particle ion cyclotron resonance and ion cyclotron heating of the plasma generated by the Joule heating in the Heliotron-B. These experiments are carried out after the investigations of plasma behaviours under the Joule heating, such as plasma current distribution in the discharge tube, electron and ion temperature, spectral lines of impurities and correction for vertical field produced by primary Joule heating currents[8,9].

2. Principle of Ion Cyclotron Heating in the Heliotron-B

The Heliotron magnetic field is generated by electric currents in a series of pair coils, when these coils are axisymmetrically wound around a discharge tube at regular intervals and the electric currents in each pair coils are different in intensity and direction. Fig. 1 shows the configuration of magnetic field produced in such a way.

A remarkable characteristic of the Heliotron field is that zero-field circles (or neutral lines: N. L.) are situated inside the discharge tube. Therefore, the magnetic lines of force can be decomposed into two groups ; those of a

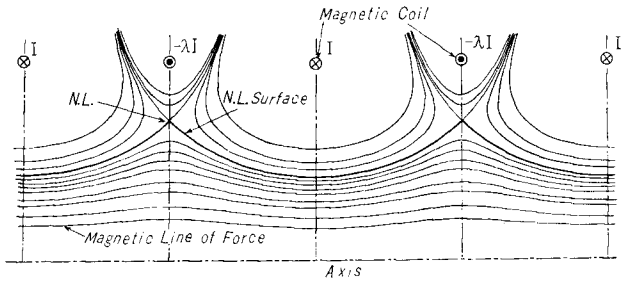

Fig. 1. Heliotron magnetic field.

group lie inside the N. L. surface and undulate along the tube axis without touching the tube wall, and those of another group lie outside the N. L. surface and certainly intersect the tube wall. If dilute plasma is inserted in this Heliotron field and *dc* electric field is applied in the axial direction, the resulting plasma current will be concentrated in the central region near the tube axis. Because charged particles of plasma inside the N. L. surface can travel and be accelerated without touching the wall surface and, as a result, these particles can generate concentrated current near the tube axis. The magnetic mirror effect of the Heliotron field also strengthens this concentrating tendency of plasma current. Thus hot plasma will be produced and confined in the Heliotron field without contact with the tube wall and its impurity level will be very low.

Experimentally, these anticipations could be verified by experiments on the Joule heating of plasma in the Helitron-B. The electron temperature of plasma could be raised to fairly high temperature of 5×10^5 °K but the ion temperature stayed within lower value around 1×10^5 °K. Spectral lines from impurities in the plasma were observed, such as O II, O III, N II, C I, C II, C III, Fe II, Cr II and Mn II, which were originated from the tube wall surface or from the back flow of oil vapour of a diffusion pump. These lines, however, were hardly perceptible in discharge in the Heliotron field. It is ascribed to the long equipartition time that the ion temperature is considerably lower than the electron temperature under the Joule heating. This time is 220μ sec. under the condition that electron tempeaature is 2×10^5 °K, ion temperature 1×10^5 °K and plasma number density 10^{13} cm^{-3}. Therefore, another heating method is needed to heat ions selectively. The Heliotron-B is equipped with ion cyclotron heating parts for the reason.

Fig. 2 shows a schematic explanation of this ion cyclotron heating mechanism. The magnetic field in the exciting region for waves is uniform

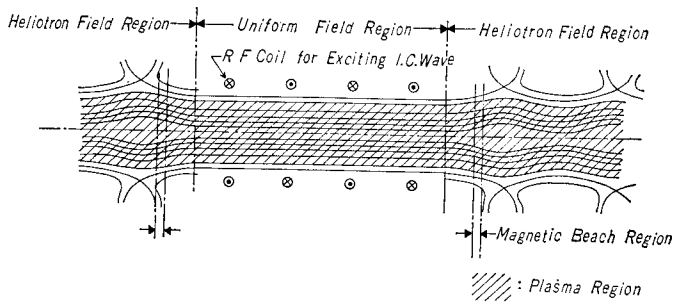

Fig. 2. Schematic explanation of exciting and damping of ion cyclotron waves in the Heliotron-B.

and continues to the Heliotron field. Thus ion cyclotron waves excited by a *rf* coil in the uniform field propagate into the Heliotron field and may be subjected to the cyclotron damping or the thermalization. Finally, ions will be heated up. The condition on the appearance of magnetic beach region is given by

$$\frac{B_{\min}}{B_0} < 1 - \frac{\omega_{pi}^2}{\kappa^2 c^2} - \frac{\omega_{pi}^2}{(\kappa^2+\nu^2)c^2}, \tag{1}$$

where $B_{\min}$ and B_0 are the minimum magnetic field of the Heliotron field and the magnetic field in the *rf* coil region, ω_{pi} ion plasma frequency, κ axial wave number, ν radial wave number and c light velocity.
Since

$$\frac{\omega_{pi}^2}{\kappa^2 c^2} \simeq 4.87\times10^{-17}\frac{Z_i^2 n_i^2}{A}\left(\frac{2\pi}{\kappa}\right)^2, \tag{2}$$

$$\nu r_p \simeq 3.83 \text{ (i. e. a principal mode of } J_1(\nu r_p) = 0)$$

and $$r_p \simeq 2\,\text{cm},$$

we have

$$\frac{B_{\min}}{B_0} < 1 - 8.4\times10^{-5} n_i, \text{ for protons.} \tag{3}$$

Where n_i, Z_i and A are ion number density, ion charge in units of proton charge and atomic weight, respectively.

In the case of the Heliotron-B, $B_{\min}/B_0 \simeq 1/4$, so that ion cyclotron waves of plasma density within $9\times10^{13}\,\text{cm}^{-3}$ may be damped during their propagation through the Heliotron field. These magnetic beach region are localized near a definite position, where frequency becomes equal to the ion cyclotron frequency. Consequently, hot ions with transverse energy, converted from the wave energy, may be trapped in the magnetic mirrors of the Heliotron field. To heat ions everywhere in the torus, it is desirable to apply a *dc*

electric field along the tube axis and to supress such a ion trapping. Some anxious phenomena may be accompanied with the *dc* application; that is, macroscopic flow of ions induced by the *dc* field may violate the wave resonant condition. However, the Heliotron-B of a race track shape has many beach regions and some extent of damping certainly occur in each beach region, so that ion cyclotron waves can be finally damped in the torus.

Plasma under Joule heating may have beam-like ions and, as a result, *rf* loading of plasma occurring from the single particle resonance of ions may appear at a shifted frequency from the ion cyclotron frequency, due to Doppler effect. If the ion beam velocity is considerably faster than the mean thermal velocity of ions, this frequency shift may be distinctly observed as demonstrated in Appendix. In this case, the associated frequency shift Δf is

$$\Delta f \simeq \frac{\kappa u}{2\pi}, \tag{4}$$

where u is the beam velocity. Experimentally, this Doppler shift can be observed as described in Section IV.

3. Heliotron-B Device with Ion Cyclotron Heating Parts

The discharge tube of the Heliotron-B is of a race track shape. It is made of stainless steel of 2 mm thickness and insulated by a ceramic tube at one of the two linear legs of the race track shape. This ceramic tube prevents the discharge tube from short-circuiting the heating transformer on the secondary side and provides a convenient section for the ion cyclotron heating. The torus radius of its curved part is 31.2 cm and the total circumference along the tube axis is 2.96 m. The inner diameter of the discharge

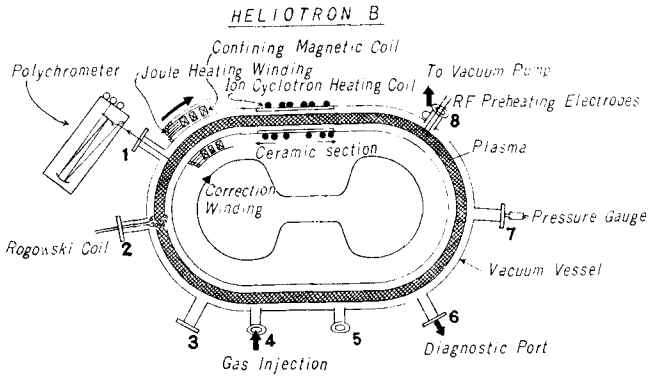

Fig. 3. Simplified schematic drawing of the Heliotron-B.

tube is 8.4 cm at the linear parts and 7.5 cm at the curved parts. The positive and negative coils, which produce the Heliotron magnetic field, are supported by the gun metal cases fixed on the angle-irons. The ratio, λ, of the current in the positive coil to that in negative coil can be adjusted to be 1 to -1, according to the purpose of experiment. For example, the case $\lambda=1/4$ corresponds to the Heliotron field and the case $\lambda=0$ or $-1/4$ does to the Bumpy torus type field[10]. A Joule heating winding, which induces the accelerating electric field, is wound outside the gun metal cases along the tube. Nine viewing ports for observation are also installed. Fig. 3 shows a simplified schematic drawing of the Heliotron-B.

Joule Heating

Pulsed confining magnetic field is used in the Heliotron-B. Energy for this field is stored in a capacitor bank of 6.4×10^4 joules. The switching is performed with an ignitron MI-1200. Subsequent to the initial *rf* breakdown of gas, the gas is brought to a fully ionized state and heated by means of a unidirectional axial electric field induced by the current in the Joule heating winding. The current is also generated by the discharge of a capacitor bank of 2×10^4 joules.

There is an inevitable defect in this heating method: the currents flowing with a certain curvature in the toroidal windings produce a magnetic field (vertical field) perpendicular to the plane of the torus. The vector force generated as the vector product of the plasma current and the vertical magnetic field pushes the plasma column to the discharge tube and disturbe the equilibrium condition of plasma confinement. The vertical field in the Heliotron-B amounts to 1.2×10^3 gausses on the axis. In order to eliminate the vertical field, the Heliotron-B is equipped with a correction winding of a dumb-bell shape as shown in Fig. 3. As a result, this vertical field can be compensated within 10 gausses over the discharge region.

Ion Cyclotron Heating

A *rf* coil for exciting ion cyclotron waves is wound around the ceramic tube and made of a gold-plated copper lod of 8 mm in diameter. It shapes so that the azimuthal direction of *rf* current alternates every 1.5 turns at the axial interval of 6 cm. Thus the coil imposes an axially periodic perturbation on plasma over a range of two wave lengths of 24 cm. The hot lead of the *rf* coil is connected to the centre tap of the coil and two ends of the coil are connected to a grounded copper tube, which forms a coaxial line with the hot *rf* lead. Polyethylene insulator filled between the leads helps

to prevent arcing at the high *rf* voltage up to 5×10^4 volts. The *rf* coil is enclosed with a stainless tube of thickhess 2 mm for *rf* shielding.

The magnetic field in the *rf* coil region was designed to be uniform by using an axially symmetric field simulator. Fig. 4 shows the arrangement of the *rf* coil, the magnetic coils, the ceramic tube and the shielding tube.

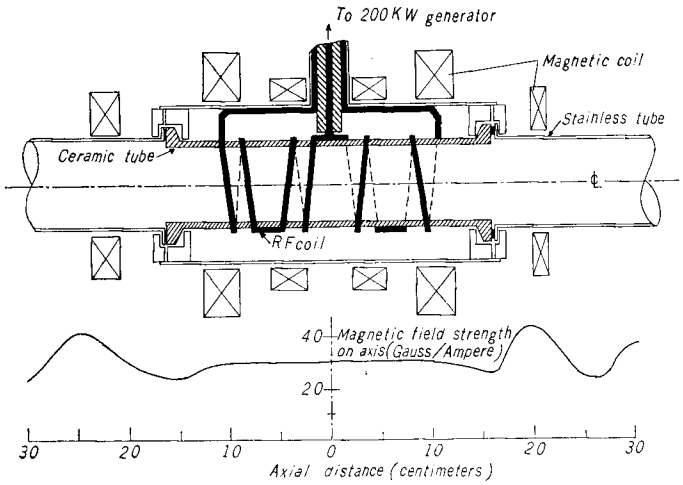

Fig. 4. Sectional diagram of the ion cyclotron heating section of the Heliotron-B device. Also shown is the magnetic field strength in the axial direction.

The *rf* coil is supplied with *rf* current from a high power pulsed *rf* generator. The coil is tuned to resonance with a capacitance network as shown in Fig. 5. The capacitors for the network are of ceramic disk type and mounted in a cylindrical brass shielding case. The pulsed *rf* generator

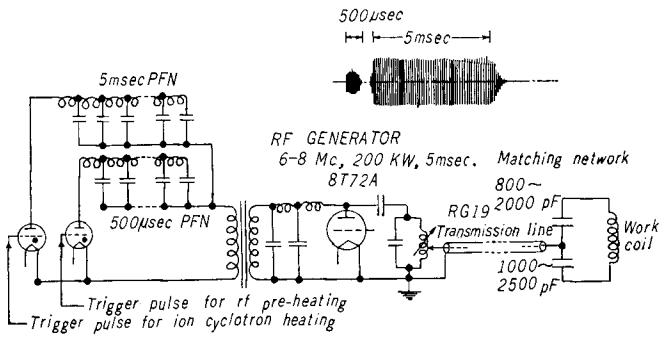

Fig. 5. Circuit diagram of the connection between the pulsed *rf* generator and the work coil for ion cyclotron heating.

is capable of 400 kW peak power over a frequency range of 6 to 8 Mc and its pulse duration is about 5 msec. In addition, another *rf* pulse of 50 kW is also generated for pre-ionization of plasma and its pulse duration is 500 μsec.

Time sequence of operation

Fig. 6 shows the block diagram of the pulse circuit for setting the time sequence of operation. At first, the magnetic coils are energized with the discharge of the capacitor bank for the magnetic field. Next, slightly before the peak of the magnetic field strength, a *rf* pulse of 1 kW 10 Mc for the

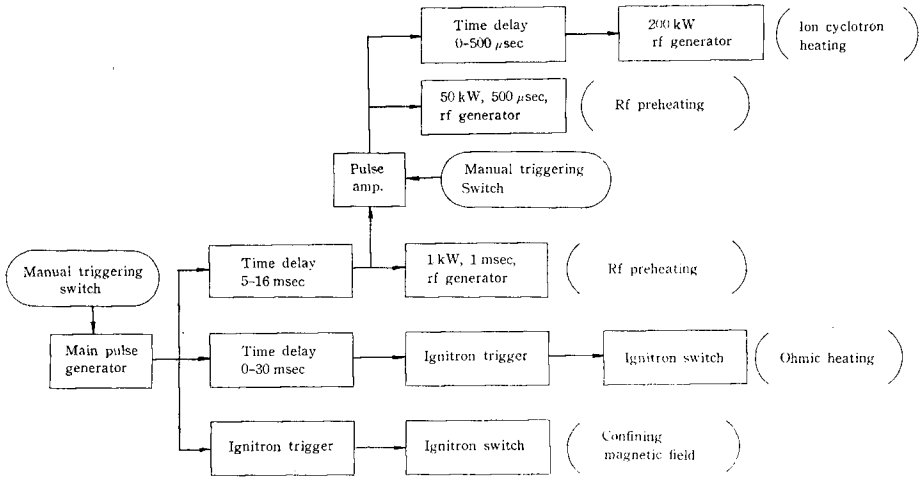

Fig. 6. Block diagram of the pulse circuit for the ion cyclotron heating in the Heliotron-B.

initial breakdown of gas and the *rf* pulse of 50 kW for pre-ionization are supplied. Then, 1 msec after, the Joule heating field is imposed. Concurrently, the plasma is excited with the pulsed high *rf* field fed from the *rf* generator. A typical schedule of the timing is shown in Fig. 7. Fig. 8 and 9 show the oscillograms of the magnetic coil current and the *rf* coil voltage.

Fig. 10 shows a photograph of the Heliotron-B attached with these ion cyclotron heating parts.

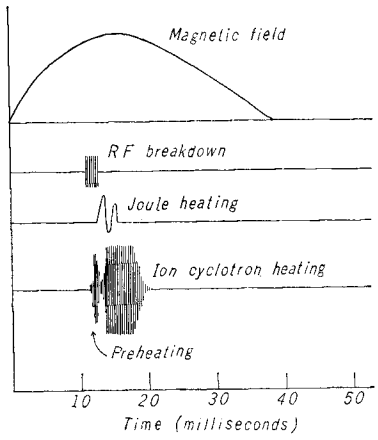

Fig. 7. Relative time sequence of the operation of the Heliotron-B.

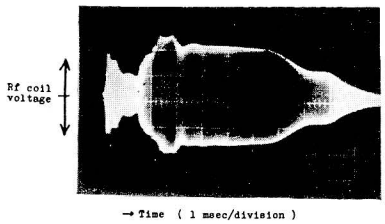

Fig. 9. Oscillogram of *rf* work coil voltage.
Vertical scale : 3.8 kV per division,
Power : 78 kW.

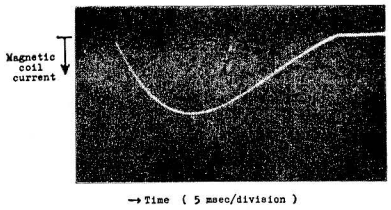

Fig. 8. Oscillogram of magnetic coil current.
Vertical scale : 100 A per division,
Magnetic field : Heliotron type ($\lambda = 1/4$),
Charged voltage of the capacitor bank : 5 kV.

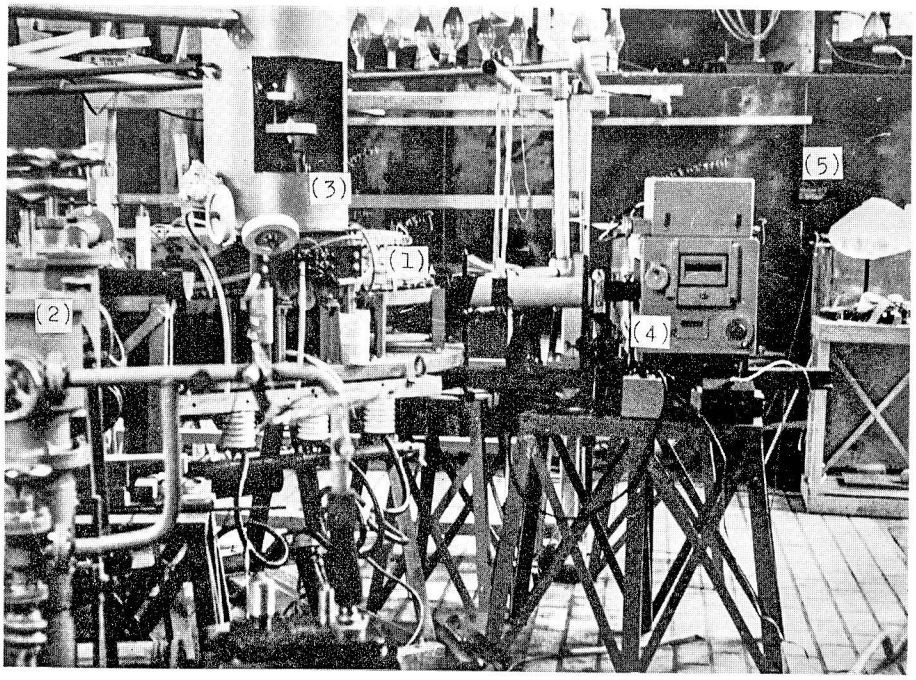

Fig. 10. Photograph of the Heliotron-B and measuring apparatus.

Plasma Diagnostics

Many diagnostic instruments are used to investigate phenomena of discharge. There are Bogowski coils for measuring the total plasma current, a double prism spectrometer for inferring the electron temperature, a plane grating spectrometer for inferring the ion temperature, a *rf* coil voltage indicator, a double turns *rf* magnetic probe for detecting the ion cyclotron waves etc..

The electron temperature of the plasma is inferred from the relative strengths of related singlet (4922 Å) and triplet (4713 Å) lines in the neutral helium spectra. This method developed by Cunningham[11] may be in error. Because Lin and St. John revealed the pressure dependence of the electron-excitation function of the 4^1D state of helium[12] However this pressure dependence of the transition to 4^1D appears distinctly at pressure above 1.4×10^{-2} Torr. At lower pressure than this value the cross section may be regarded constant. On the other hand, the 2^3P–4^3S transition (4713 Å) is relatively insensible to pressure in the range of 0 to 1.3×10^{-1} Torr. The helium gas pressure in this experiment is in a range of 2×10^{-4} to 5×10^{-4} Torr. Therefore, the pressure dependence of the excitation cross section will be negligible, so that electron temperature of plasma in this experiment can be determind from the intensity ratio of HeI 4922 to HeI 4713 lines. Sovie[13] proposed a refinement of the method of Cunningham from the intensity ratio of HeI 5047 to HeI 4713, in consideration of the insensible property to pressure of 2^1P–4^1S transition (5047 Å). This line is, however, so weak in this experiment that its S/N ratio would not be good. Ten percents of helium is mixed in hydrogen gas to detect the helium lines.

The ion temperature of plasma is inferred from the Doppler broadenings of spectral lines of ionized atoms. In this experiment, a singly ionized helium line HeII 4686 Å is very weak, so that exposures of 400 times are needed to take only a spectrogram of the line. A singly ionized carbon line CII 4267 Å as an impurity line is detected for this purpose, owing to its strong intensity. Multiple ionized lines would be more suitable but these lines are too weak to be detected in this case. The equipartition time, t_{eq}, between protons and singly ionized carbon atoms becomes about 56 μ sec under the condition that proton temperature is 2×10^5 °K, proton number density 10^{13} cm^{-3} and the temperature of singly ionized carbon atoms 10^4 K°. The time is sufficiently short compared with the heating time duration, that is 1 msec for the Joule heating and 5 msec for the ion cyclotron heating. Therefore, the sufficient equipartition between C^+ and H^+ may be achieved. Under the condition that magnetic field is 1000 gausses and the energy of C^+ is 20 eV, the Larmar radius of C^+ becomes 2 cm. The inner tube diameter and the minimum magnetic field strength on the axis of the Heliotron-B are 8 cm and about 1000 gausses. Furthermore, the averaged minimum field over the radii is weaker. Thus the upper limit of ion temperature observable by using C^+ line is about 4×10^5 °K. The Stark broadening of CII 4267 Å is approximately of the order of 10^{-5} in angström units, which is negligible compared with

the resolvable line width of the spectrometer or the Doppler broadening width of C^+ line.

4. Preliminary Experiment on RF Absorption of Plasma

Plasma density produced in the Heliotron-B is attainable to fairly high value as $10^{14}\,cm^{-3}$, so that the *rf* absorption resulting from the excitation of ion cyclotron waves is expected to be clearly distinguished from the single-particle cyclotron resonance absorption. This separation will give a clear evidence for the existence of ion cyclotron waves in plasma. The experiment described in this section is carried out so as to get basic and preliminary information on the ion cyclotron heating of plasma in the Heliotron-B. Namely, the efficiency for exciting the waves, the existence of ion beams and other cooperative phenomena are investigated.

Experimental Procedure

The detecting method of *rf* absorption of plasma belongs to a frequency sweeping (or plotting) type. A Franklin oscillator is used[14], since it has a pure sinusoidal wave form and can cover the wide frequency range with little variation of its power. The resonant circuit of the oscillator consists of inductance L_w (*rf* work coil) and L_a (auxiliary coil), and a capacitor. Its oscillating power is about 40 mW in the present case. The power absorption of plasma from the *rf* field induced by L_w can be detected by measuring the variation of oscillating level of the oscillator at each given frequency. The auxiliary coil L_a is used for preventing a frequency shift under plasma loading. The absolute power absorption can be obtained from the calibration of dissipated power for many different frequencies and loads by changing the oscillator frequency and damy load. Frequency shift caused by plasma reaction is within 1×10^{-3} at 3.5 Mc and 8×10^{-3} at 7.5 Mc. The frequency range is from 3 to 15 Mc.

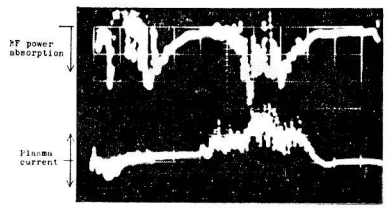

Fig. 11. Oscillogram of the signals of *rf* power absorption obtained from the Franklin type oscillator and plasma current during the Joule heating.
Gas : Deuterium, $p_0=4.4\times10^{-3}$ Torr (D_2),
Magnetic field in the *rf* coil reglon : 7300 G,
Rf frequency : 9.60 Mc,
Scan speed : 100 μ sec/division.

If the reproducibility of the plasma produced by each Joule heating is mostly perfect, the power absorption curve (or efficiency curve of the absorption) at any given

time after the start of the Joule heating can be obtained by plotting the power absorption (or efficiency) against each given frequency. Representative oscillograms of the *rf* absorption signal and the total plasma current are shown in Fig. 11.

Experiments are carried out for hydrogen, helium and deuterium discharges. Magnetic field used are the Heilotron type ($\lambda=1/4$) and the Bumpy torus type ($\lambda=-1$ or $-1/2$). The correction winding is not working unless otherwise noted.

Hydrogen Discharge

Oscilloscope traces of typical *rf* absorption signals in hydrogen discharge are shown in Fig. 12, where f_{ci} denotes the ion cyclotron frequency in the magnetic field, B_0, in the *rf* coil region, E_J the maximum Joule heating field

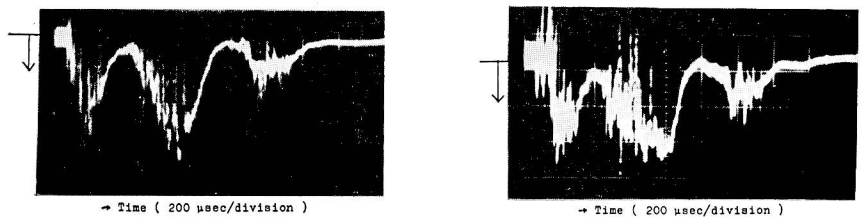

(a) (b)

Fig. 12. Oscillograms of the signal of *rf* power absorption in hydrogen plasma for two different frequencies.
Magnetic field : Heliotron type ($\lambda=1/4$),
$B_0=6500$ G, $E_J=1.6$ V/cm,
$p_0=1\times10^{-3}$ Torr (H_2).
(a) $f=8.8$ Mc ($=0.88\ f_{ci}$).
(b) $f=10.5$ Mc ($=1.05\ f_{ci}$).

and p_0 the initial gas pressure. The absorption signals are pretty noisy. This noise is thought to originate in plasma oscillations, which are also observed with a stream camera. The *rf* power absorption peak almost arises at the peak of the plasma current. From these signal amplitudes as a function of the frequency, the existence of ion cyclotron waves and the heating efficiency can be inferred.

Fig. 13 shows a representative plotting of the signal amplitude against the *rf* frequency. There appear two kinds of peaks; one peak indicated by S is lying near f_{ci}, and the other peak indicated by W is at 10 Mc, which is lower frequency than f_{ci}. Furthermore, the peak S appears on both sides of f_{ci} and its frequency deviation from f_{ci} depends on the time of observation after the start of the Joule heating. These facts suggest that the peak S

corresponds to the absorption resulting from single-particle cyclotron resonance and shifts with a Doppler effect predicted in Section II. On the other hand, the peak W is thought to originate in the absorption due to the excitation of the ion cyclotron wave. The frequency shift of the peak W from f_{ci} is nearly constant at the time range of 550 to 800μ sec after the Joule ignition. Therefore, the plasma density may be considered to be nearly constant during the time as seen in the dispersion relation of ion cyclotron waves. In somewhat higher Joule heating field, the peak S is no longer clearly observed, as seen in Fig. 14. This extinction of S is perhaps due to the occurence of many ion beams in the plasma and, as a result, any distinctive peak S can hardly appear. These discussions of ion

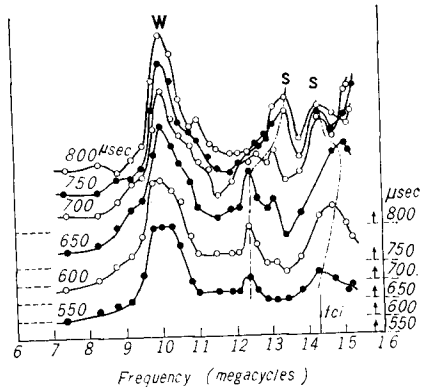

Fig. 13. Frequency dependences of the signal amplitude of *rf* power absorption at various times after the ignition of Joule heating. Zero-level of each signals by a broken line, on which the corresponding time is noted.

Magnetic field : Heliotron type ($\lambda=1/4$), $B_0=9370$ G, $E_J=1.2$ V/cm, Gas : hydrogen, $p_0=1.2\times10^{-2}$ Torr.

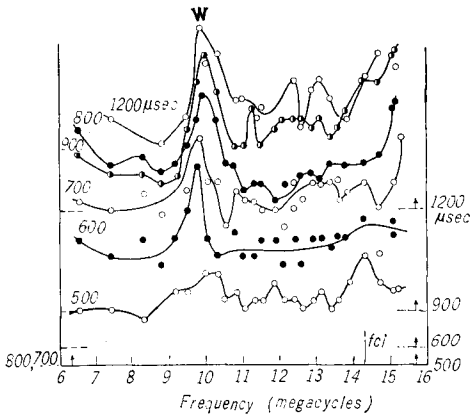

Fig. 14. Frequency dependences of the signal amplitude of *rf* power absorption at various times after the ignition of Joule heating.

Magnetic field : Heliotron type ($\lambda=1/4$), $B_0=9370$ G, $E_J=1.7$ V/cm, Gas : hydrogen, $p_0=1.2\times10^{-2}$ Torr.

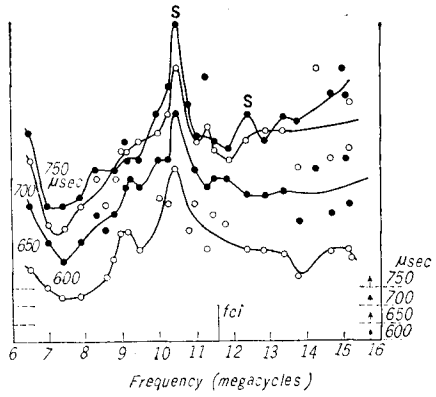

Fig. 15. Frequency dependences of the signal amplitude of *rf* power absorption at various times after the ignition of Joule heating.

Magnetic field : Heliotron type ($\lambda=1/4$), $B_0=7540$ G, $E_J=1.2$ V/cm, Gas : hydrogen, $p_0=1.2\times10^{-2}$ Norr.

beams, however, are applicable only to the plasma near the surface, since the single-particle cyclotron resonance at considerably higher plasma density can occur only in the surface region because of the shielding reaction of ion currents against the *rf* field. On the contrary, the peak W can be clearly seen even in Fig. 14. At a lower magnetic field, the single-particle resonance curve is also observed near the *rf* frequency of f_{ci}, whereas the peak W shifts left and can not be observed. Fig. 15 shows the case of this lower magnetic field.

From the dispersion relation of ion cyclotron waves and the experimentally obtained frequency shift of the peak W from f_{ci}, we can infer the plasma density. Table 1 shows plasma densities obtained in such a way for different cases. Here, the dispersion relation used is for cold plasma with axisymmetric modes. Calculated plasma densities on the assumption of full ionization of the initially charged neutral gas are also given for comparison. The initial atom number density is usually greater than the density obtained from the frequency shift. This tendency is roughly verified from the mesurement of plasma density with a Langmuir double probe. A simple interpretation of the difference between $n_{i\,\mathrm{cal}}$ and $n_{i\,\mathrm{obs}}$ in Table 1 is that a part of the neutral gas is pumped out to the region outside the N.L. surface before atoms are ionized. Similar phenomena were observed by Stix and Palladino in the experiments on the B-65 Stellarator[15]. According to their report, 80~90% of the neutral gas (D_2) was pumped out to the wall during the ionization process. However, this disparity is smaller in the case of the Heliotron-B. A cause for it is thought to be that the gas molecules outside the N.L. surface incessantly flow into the region inside the surface, where the plasma current is flowing and ionization is progressing. The plasma density, therefore, can be apparently retained in some extent.

Table 1. Comparison between the plasma density obtained from the frequency shift and that from the fully ionizing assumption.

Initial gas pressure Torr (H_2)	$n_{i\,\mathrm{cal}}$* cm^{-3}	$n_{i\,\mathrm{obs}}$** cm^{-3}	$n_{i\,\mathrm{obs}}/n_{i\,\mathrm{cal}}$
1.9×10^{-2}	1.3×10^{15}	1.8×10^{14}	1.4×10^{-1}
1.2×10^{-2}	8.5×10^{14}	2.2×10^{14}	2.6×10^{-1}
1.2×10^{-2}	8.5×10^{24}	1.9×10^{14}	2.2×10^{-1}
7.2×10^{-3}	5.0×10^{14}	3.8×10^{14}	7.6×10^{-1}
6.0×10^{-3}	4.2×10^{14}	3.9×10^{14}	9.3×10^{-1}

* Ion density calculated on the assumption that initially immersed neutral gas is fully ionized.

** Ion density obtained from the frequency shift of the absorption peak from the ion cyclotron frequency, where the radial wave number is assumed to be $2.0\,\mathrm{cm}^{-1}$.

In order to indicate the efficiency of the *rf* absorption of plasma, let a measure α defined as

$$\alpha = \frac{\text{Power absorbed by plasma}}{\text{Power lost in the } rf \text{ system}}. \qquad (5)$$

Fig. 16(a) shows the amplitudes of signal of the absorption versus *rf* frequency in a wide frequency range, and the associated α curves are shown in Fig. 16 (b). The peak W does not distinctly separate from the peak S. There also appears a peak near a half of proton cyclotron frequency, maybe caused from H_2^+ cyclotron resonance.

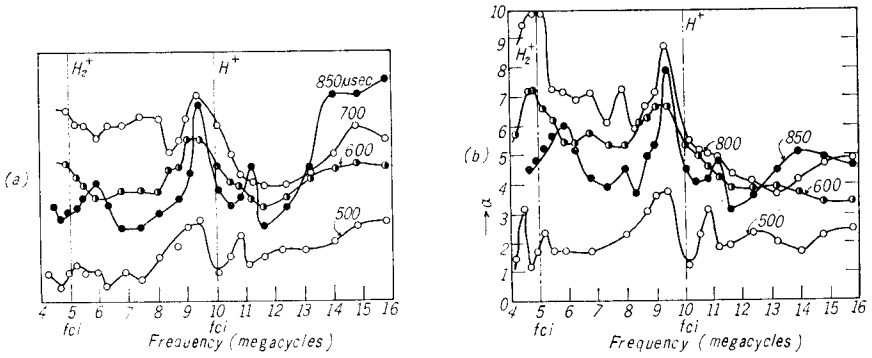

Fig. 16. Amplitudes of the *rf* absorption signal and the corresponding α curves as a function of *rf* frequency.
Magnetic field : Heliotron type ($\lambda=1/4$),
$B_0=6500$ G, $E_J=1.2$ V/cm, Gas : hydrogen,
$p_0=7.2\times10^{-3}$ Torr.
(a) Amplitude of the absorption.
(b) α values.

To see minutely α curves near the cyclotron frequency, representative α curves obtained in a narrow frequency range are shown in Figs. 17 and 18. An asymmetry of the α curve arises on the lower frequency side from f_{ci}, and the extent of the asymmetry increases as the initial gas pressure becomes higher. This asymmetry is due to the excitation of the ion cyclotron waves for considerably lower density plasma, as observed by Stix and his collaborators.

Thus it becomes evident that the existence of ion cyclotron waves can be indirectly proved from the asymmetry or the frequency shift of α curves and the efficiency to excite the wave is about 75%.

Rf absorption curves have double peak S on the both sides of the ion cyclotron frequency and corresponding beam velocity can be determined from equation (4). The result is summarized in Table 2.

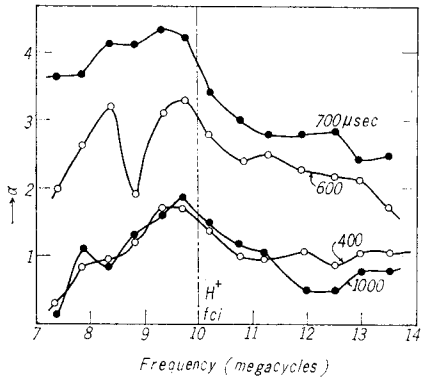

Fig. 17. α as a function of rf frequency at various times after the ignition of Joule heating.

Magnetic field Heliotron type ($\lambda=1/4$), $B_0=6500$ G, $E_I=1.3$ V/cm, Gas : hydrogen, $p_0=7\times10^{-3}$ Torr.

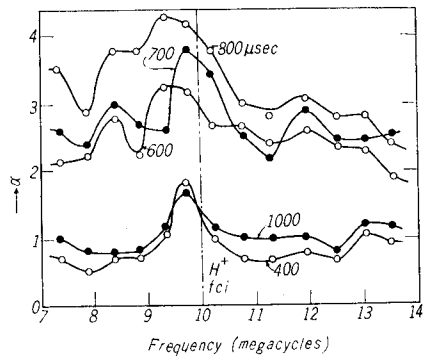

Fig. 18. α as a function of rf frequency at various times after the ignition of Joule heating.

Magnetic field : Heliotron type ($\lambda=1/4$), $B_0=6500$ G, $E_I=1.3$ V/cm, Gas : hydrogen, $p_0=3\times10^{-3}$ Torr.

Helium Discharge

For experiments on the excitation of ion cyclotron waves of doubly ionized helium, He^{++}, it is required that sufficient ionization of helium gas is attainable during the Joule heating. Namely, the electron temperature must be pretty high to produce doubly ionized helium atoms. A check on the completeness of ionization is experimentally made by observing the spectral lines of singly ionized atoms, He^{+}. If the intensities of spectral lines of He^{+} are sufficiently strong, one can expect large abundance of He^{++} in plasma. Fig. 19 shows a typical microphotometric trace of the time-integrated spectrogram, where the $\lambda=1/4$ Heliotron field is used. A singly ionized helium line, HeII 4686 Å, is imperceptible, while neutral helium lines are very strong in intensity. The viewing port for observation is **1** in Fig. 3, so that it can not immediately be concluded that there is no He^{++} in the rf coil region. But its concentration is never large. As the total plasma current is about 3000 A in this case, more ionization will be achieved with the increase of the plasma current by using the Bumpy torus type field ($\lambda=-1/2$). Fig. 20 shows the microphotometric trace in the case of the Bumpy torus field, where the plasma current is about 5000 A. Weak HeII 4686 line is perceptible. Therefore, He^{++} may be also produced to some extent.

(i) Discharge in the Bumpy torus field

Fig. 21 and 22 show examples of α curve for different initial pressures in the Bumpy torus type field ($\lambda=-1/2$). Doppler shifted peaks S due to

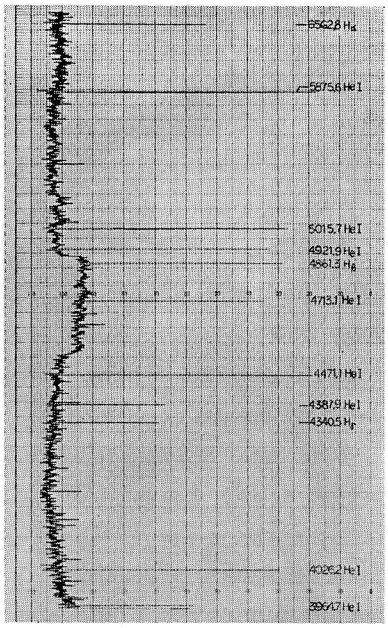

Fig. 19. Typical microphotometric trace of the time-integrated spectrogram of plasma under the Joule heating.

Magnetic field : Heliotron type ($\lambda=1/4$), $B_0=8100$ G, $E_J=1.2$ V/cm, Gas : helium, $p_0=8.8\times10^{-3}$ Torr.

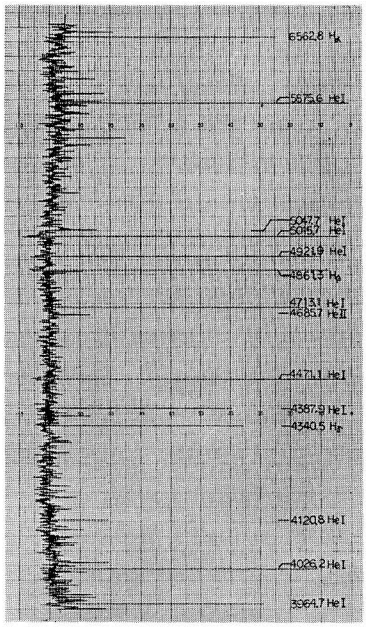

Fig. 20. Typical microphotometric trace of the time-integrated specrogram of plasma under the Joule heating.

Magnetic field : Bumpy torus type ($\lambda=-1/2$), $B_0=6340$ G, $E_J=1.0$ V/cm, Gas : helium, $p_0=1.2\times10^{-2}$ Torr.

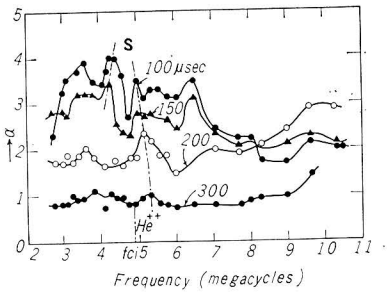

Fig. 21. α as a function of *rf* frequency at various times after the ignition of Joule heating.

Magnetic field : Bumpy torus type ($\lambda=-1/2$), $B_0=6340$ G, $E_J=1.0$ V/cm, Gas : helium, $p_0=5.4\times10^{-2}$ Torr (He).

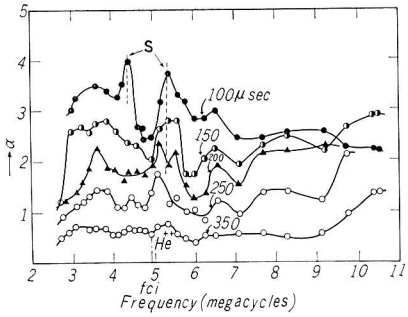

Fig. 22. α as a function of *rf* frequency at various times after the ignition of Joule heating.

Magnetic field : Bumpy torus type ($\lambda=-1/2$), $B_0=6340$ G, $E_J=1.0$ V/cm, Gas : helium, $p_0=3.0\times10^{-2}$ Torr (He).

single-particle cyclotron resonance of He^{++} appear in both figures. These shifts are clearly perceptible and large, immediately after the ignition of the Joule heating (see the α currves at 100μ sec). Other many peaks are also present and some of them are probably due to the existence of other He^{++} beams. Ion cyclotron waves are not excited probably, because of the little abundance of He^{++}.

(ii) Discharge in the Heliotron type field

Though He II 4686 line is imperceptible from the viewing port **1**, the peak S appears in α curves in practice. Its Doppler shift is fairly large in comparison with those in the case of the Bumpy torus field. Some examples of α curves are shown in Figs. 23 and 24, where the curves correspond to the second peak of the plasma current. In a given Joule heating field, on the whole, the Doppler shift at higher initial pressure (Fig. 23) is smaller than that at lower initial pressure (Fig. 24). The fact is perhaps due to the different mean free path lengths of He^{++} in the plasma for different pressure.

The *rf* absorption efficiency in the case of the Bumpy torus field is better than that in the case of the Heliotron field, that probably arises from the difference of the He^{++} density. From the same reason, α value for H^{+} in hydrogen discharge is greater than for H^{++} in helium discharge.

A probable explanation of these large shifts of the peak S of α curves may be considered. The magnetic lines of force near the inner surface of the ceramic tube intersect with the stainless tube wall due to the undulation of the Heliotron field, so that charged particles moving along these lines

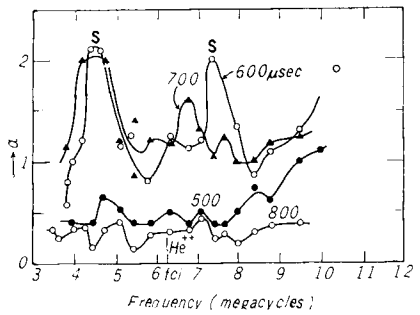

Fig. 23. α as a function of *rf* frequency at various times after the ignition of Joule heating.

Magnetic field : Heliotron type (λ=1/4). B_0=8100 G, E_r=1.3 V/cm, Gas : helium, p_0=1.6×10^{-2} Torr (He).

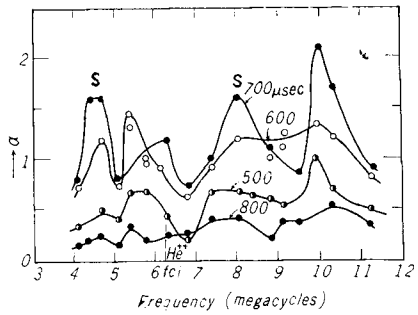

Fig. 24. α as a function of *rf* frequency at various times after the ignition of Joule heating.

Magnetic fields : Heliotron type (λ=1/4), B_0=8100 G, E_r=1.3 V/cm, Gas : helium, p_0=8.8×10^{-3} Torr.

directly short the both sides of the stainless tube. During the Joule heating, the voltage between both ends of the stainless tube is very high (average 250 V). Therefore, these particles can get high energy during the shortening and also ionization of helium to He^{++} is progressing in this region. Many shortening region may appear and may be strengthened with the bending of the lines of force by the vertical field produced by the Joule heating primary current. Table 2 gives the ion beam velocities determined from equation (4).

Table 2. Ion beam velocities determined from the Doppler shift of α curve under various conditions.

Type	Gas	p_0 Torr	B_0 gauss	E_J V/cm	t μsec	u cm/sec	$Mu^2/2$ eV	V_L V
Hel	H_2	1.2×10^{-2}	9370	1.2	550	1.3×10^{7}	85	360
					600	1.4×10^{7}	100	
					650	1.5×10^{7}	120	
					700	7×10^{6}	25	
					750	6×10^{6}	18	
					800	5×10^{6}	13	
Bumpy	He	5.4×10^{-2}	6340	1.0	100	3.3×10^{6}	22	300
					150	4.8×10^{6}	46	
Bumpy	He	3.0×10^{-2}	6340	1.0	100	5.9×10^{6}	70	300
						9.5×10^{6}	180	
Bumpy	He	1.2×10^{-2}	6340	1.4	100	2.1×10^{6}	8	420
						5.7×10^{6}	64	
						1.0×10^{7}	200	
					150	2.1×10^{6}	8	
						1.2×10^{7}	280	
					200	2.1×10^{6}	8	
						9.5×10^{6}	180	
Hel	He	1.6×10^{-2}	8100	1.3	600	8.4×10^{6}	128	390
					800	6.0×10^{6}	72	
Hel	He	8.8×10^{-3}	8100	1.3	500	6×10^{6}	72	390
					600	9×10^{6}	160	
					700	1.1×10^{7}	240	

Hel : Heliotron type field,
Bumpy : Bumpy torus type field,
p_0 : Initial gas pressure,
B_0 : Magnetic field strength in the *rf* coil region,
E_J : Maximum Joule heating field $= V_L/300$ cm,
V_1 : Maximum loop voltage for the Joule heating,
t : Time after the ignition of the Joule heating,
M : Mass of ion,
u : Beam velocity.

Deuterium Discharge

Figs. 25 and 26 show α curves in the case of deuterium discharge in the Heliotron field.

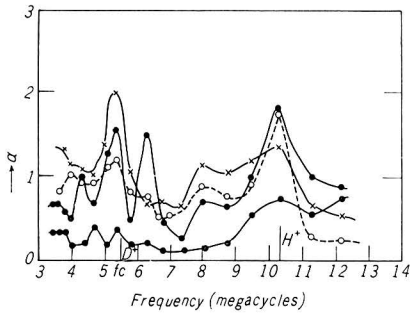

Fig. 25. α as a function of rf frequency at various times after the ignition of Joule heating.

Magnetic field : Heliotron type ($\lambda=1/4$), $B_0=7100$ G, $E_J=1.0$ V/cm, Gas : deuterium, $p_0=4.4\times10^{-3}$ Torr (D_2).

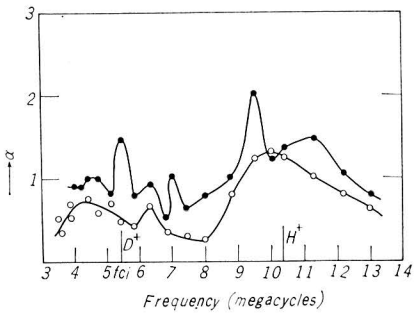

Fig. 26. α as a function of rf frequency at various times after the ignition of Joule heating.

Magnetic geld : Heliotron type ($\lambda=1/4$), $B_0=7100$ G, $E_J=1.0$ V/cm, Gas : deuterium, $p_0=8.8\times10^{-3}$ Torr (D_2).

Hydrogen Discharge under the Correction for the Joule heating Winding

Fig. 27 shows an example of the rf absorption signals when the correction winding is working. The S/N ratio is much improved compared with that without the correction (see Fig. 12). A typical α curve is shown in Fig. 28. Large shift of the peak S is no longer recognizable and a clear peak W

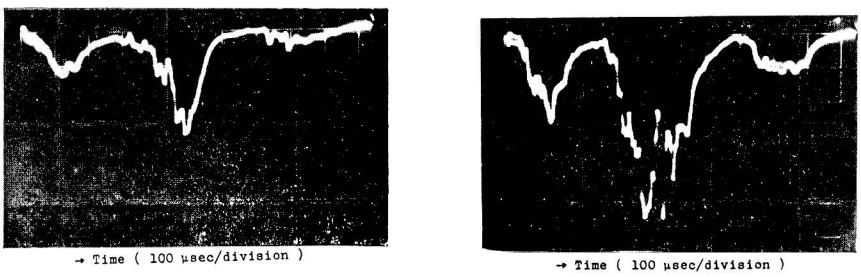

(aq (b)

Fig. 27. Oscillograms of the rf absorption signal in hydrogen plasma obtained with the Franklin type oscillator for two different frequencies. In this case, the correction winding is working.

Magnetic field : Heliotron type ($\lambda=1/4$),
$B_0=5590$ G, $E_J=1.0$ V/cm,
$p_0=2.2\times10^{-3}$ Torr (H_2).
(a) $f=4.0$ Mc ($=0.48\ f_{ci}$).
(b) $f=6.3$ Mc ($=0.73\ f_{ci}$).

shifting from f_{ci} can be seen.

Therefore, it can be said that some oscillations in the plasma and the genesis of ion beams are caused by this vertical magnetic field.

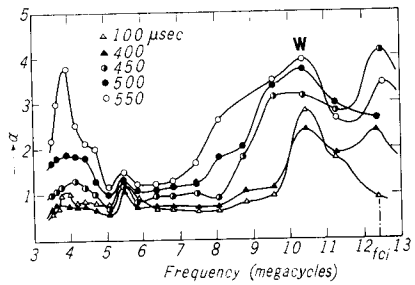

Fig. 28. α as a function of *rf* frequency at various times after the ignition of Joule heating. In this case, the correction winding is working.

Magnetic field : Heliotron type ($\lambda=1/4$), $B_0=8050$ G, $E_J=1.0$ V/cm, Gas : hydrogen, $p_0=4.4\times10^{-3}$ Torr (H_2).

5. Experiment on Ion Cyclotron Heating with High Power RF Generator

In this section, experiment on the ion cyclotron heating with the high *rf* power is described. Principal variables are the value of the confining field, the initial gas pressure and the output power of the *rf* generator. Observed properties of plasma are the propagation of ion cyclotron waves through various types of confining field, electron temperature, ion temperature and spectral lines of neutral atoms. The correction winding for the primary current of Joule heating is working through this experiment.

RF Coil Voltage and Magnetic Probe Signal

The magnetic field for plasma confinement rapidly decreases away from the *rf* coil region, so that the excited ion cyclotron waves may be immedialtely damped in the vicinity of the *rf* coil region, even in the case of the Bumpy torus field. Therefore, the excited waves will not be detected at the port **1** position.

In practice, the waves can not be detected at the port **1** position. Speaking in detail, amplitudes of the *rf* signal measured at port **1** has not any distinct peak near the cyclotron resonant field. On the other hand, the resonant absorption due to the excitation of the waves can be observed as described in the previous section. Thus it may be expect that the excited ion cyclotron waves in the *rf* coil region

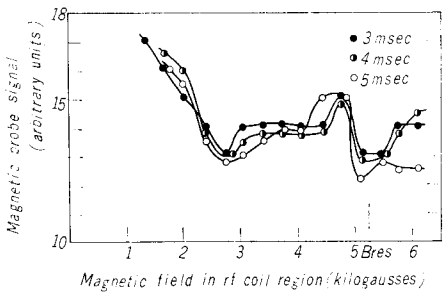

Fig. 29. Amplitude of the *rf* probe signal as a function of the field strength in the *rf* coil region at three different times after the *rf* triggering.

Magnetic field from the *rf* coil region to the probe : Bumpy torus type ($\lambda=0$), $P_{rf}=73$ kW, $f=8.1$ Mc, $p_0=2\times10^{-3}$ Torr (H_2).

are damped during their propagation to the port 1 position. Fig. 29 shows an example of the curves of the *rf* signal versus the magnetic field in the *rf* coil region, where P_{rf} and f are the *rf* power of the generator and its frequency.

Electron Temperature under the Ion Cyclotron Heating

Effects of the ion cyclotron waves upon the electron temperature may arise from the induced axial electron flow in the waves or from the relaxation between heated ions and electrons in the beach region. If the Joule heating is overlapped on the ion cyclotron heating, these effects will be veiled under the heating effect of the Joule heating itself. Because the equipartition time between ions and electrons is fairly long compared with that of electron-electron interaction. For instance, this time becomes about 220 μ sec for ion-electron interaction under the condition that plasma density is $10^{13}\,cm^{-3}$, electron temperature and ion temperature are 2×10^5 °K and 1×10^6 °K. While the time for electron-electron interaction is 0.23 μ sec under the same condition. The electron flow induced by the waves is also negligible in comparison with the Joule heating current.

(i) Electron temperature in the Heliotron type magnetic field

The magnetic field strength in the *rf* coil region is first set twice as strong as shown in Fig. 4, in order to survey the electron temperature over a wide range of the magnetic field. Fig. 30 shows examples of the oscillogram of intensities of HeI 4713 and HeI 4922 lines for different pressures. Fig. 31 shows the time variations of electron temperature for different magnetic field strengths, where the time variation of the total plasma current

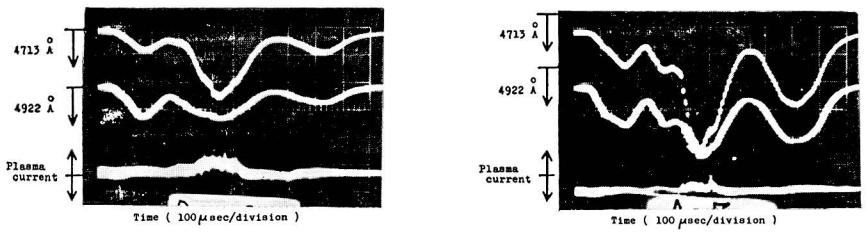

(a) (b)

Fig. 30. Oscillograms of photomultiplier signals of HeI 4713 and KeI 4922 lines and Rogowski signal of total plasma current for different two pressures.

Magnetic field : Heliotron type ($\lambda=1/4$),
$B_0=6780$ G, $P_{rf}=80$ kW, $f=8.1$ Mc.
(a) $p_0=3.6\times10^{-4}$ Torr (H_2) $+5\times10^{-4}$ Torr (He).
(b) $p_0=6.0\times10^{-3}$ Torr (H_2) $+5\times10^{-4}$ Torr (He).

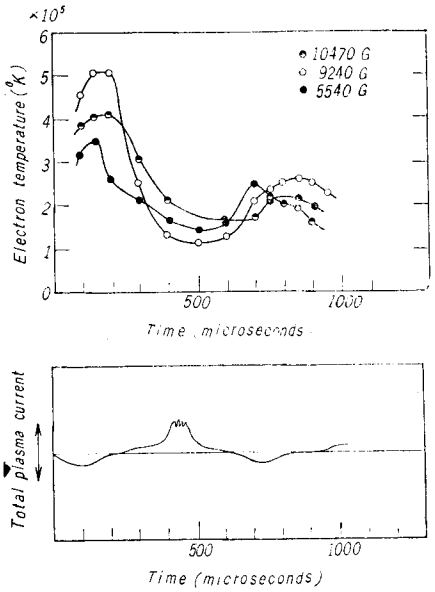

Fig. 31. Time variations of electron temperature and total plasma current for various field strengths in the *rf* coil region.

Magnetic field : Heliotron type ($\lambda=1/4$), $P_{rf}=80$ kW, f=8.1 Mc,
p_0 $=3.6\times10^{-3}$ Torr $(H_2)+5\times10^{-4}$ Torr (He).

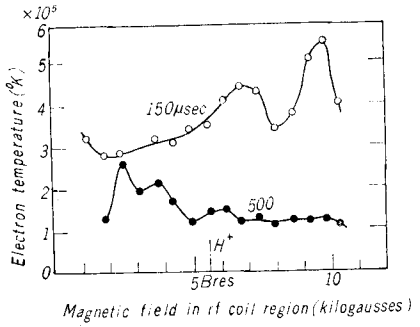

Fig. 32. Electron temperature as a function of the field strength in the *rf* coil region at different tims after the *rf* triggering. The condition is the same as in Fig. 31.

is also shown. The dependence of electron temperature on the magnetic field is shown in Fig. 32. No distinct peak near the resonant field, B_{res}, appears at any time after the start of the *rf* heating. Figs. 33 and 34 show another case at a

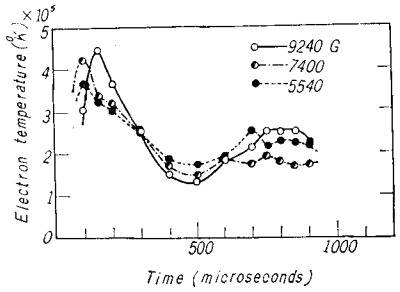

Fig. 33. Time variation of electron temperature for various field strengths in the *rf* coil region.

Magnetic field : Heliotron type ($\lambda=1/4$), $P_{rf}=80$ kW, $f=8.1$ Mc,
p_0 $=6\times10^{-3}$ Torr $(H_2)+5\times10^{-4}$ Torr (He).

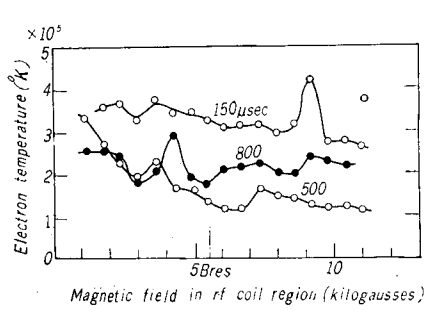

Fig. 34. Electron temperature as a function of the field strength in the *rf* coil region at various times after the *rf* triggering. The condition is the same as in Fig. 33.

higher pressure. It can be said that the effect of the ion cyclotron heating on electron temperature is not observed.

These results indicate that the electron temperature of the plasma is pretty dependent on the sense of the plasma current. This fact is probably

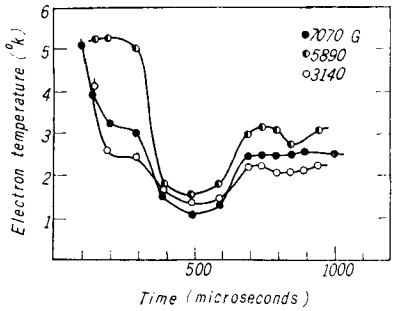

Fig. 35. Time variation of electron temperature for various field strengths in the *rf* coil region.

Magnetic field : Heliotron type ($\lambda=1/4$), $P_{rf}=73$ kW, $f=8.1$ Mc,
p_0 $=2\times10^{-3}$ Torr (H_2)$+5\times10^{-4}$ Torr (He).

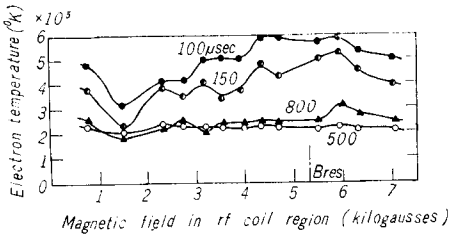

Fig. 36. Electron temperature as a function of the field strength in the *rf* coil region at various times after the *rf* triggering. The condition is the same as in Fig. 35.

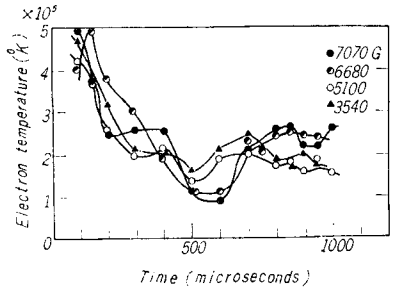

Fig. 37. Time variation of electron temperature for various field strengths in the *rf* coil region.

Magnetic field : Heliotron type ($\lambda=1/4$), $P_{rf}=73$ kW, $f=8.1$ Mc,
p_0 $=6\times10^{-3}$ Torr (H_2)$+2\times10^{-4}$ Torr (He).

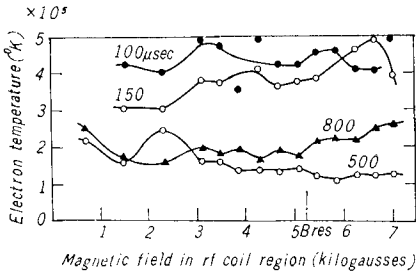

Fig. 38. Electron temperature as a function of the field strength in the *rf* coil region at various times after the *rf* triggering. The condition is the same as in Fig. 37.

caused by the lack of uniformity of the Joule heating field and by the imperfection of correction for the vertical magnetic field.

Next, the magnetic field is set as shown in Fig. 4. Time variations and field dependences of electron temperature are shown in Figs. 35 to 38.

The peak of electron temperature is situated in the first stage of the Joule heating. This fact probably originates in that the vertical field or other irregular fields generated by the primary Joule heating current is still weak in the first stage and, as a result, most of the magnetic lines of force inside the N.L. surface can close themselves along the torus, when electrons are easily accelerated.

(ii) Electron temperature in the Bumpy torus type magnetic field

Electron temperature in the case of the Bumpy torus field under different

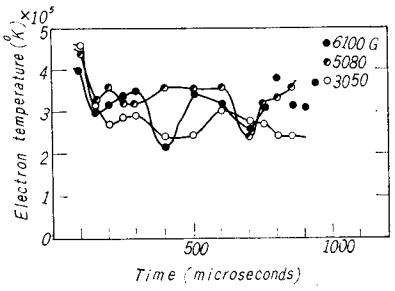

Fig. 39. Time variation of electron temperature for various field strengths in the *rf* coil region.

Magnetic field : Bumpy torus type ($\lambda=-1/2$),
$P_{rf}=73$ kW, $f=8.1$ Mc,
$p_0=3\times10^{-3}$ Torr (H_2)$+2\times10^{-4}$ Torr (He).

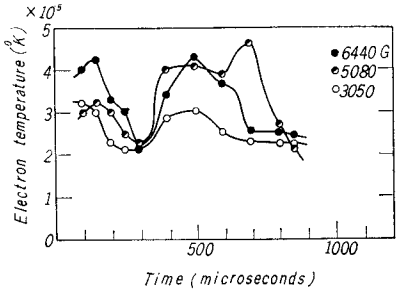

Fig. 41. Time variation of electron temperature for various field strengths in the *rf* coil region.

Magnetic field : Bumpy torus type ($\lambda=-1/2$),
$P_{rf}=73$ kW, $f=8.1$ Mc,
$p_0=6\times10^{-3}$ Torr (H_2)$+2\times10^{-5}$ Torr (He).

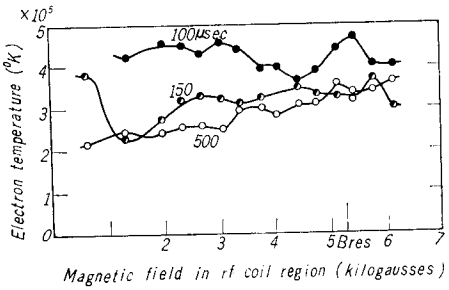

Fig. 40. Electron temperature as a function of the field strength in the *rf* coil region at different times after the *rf* triggering. The condition is the same as in Fig. 39.

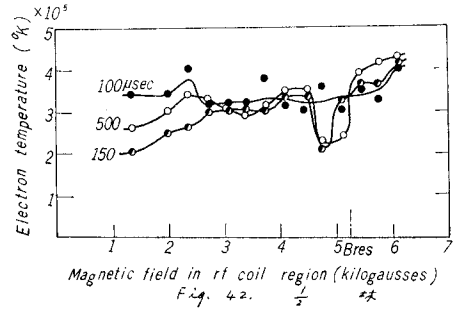

Fig. 42. Electron temperature as a function of the field strength in the *rf* coil region at different times after the *rf* triggering. The condition is the same as in Fig. 41.

conditions are shown in Figs. 39 to 42. The dependence of electron temperature on the direction of the plasma current does not clearly appear. This is due to the decrease of the bending of magnetic lines of force toward the tube wall in the strong magnetic field. No electron temperature peak near B_{res} can also be observed.

(iii) Electron temperature for different output powers of the *rf* Generator

Fig. 43 shows time variations of electron temperature for various powers of the *rf* generator at a magnetic field of 9860 gausses, where the Heliotron type field is used. A conclusion from these results is that the electron temperature is apparently insensible to the *rf* field for the ion cyclotron heating, as seen in Fig. 44.

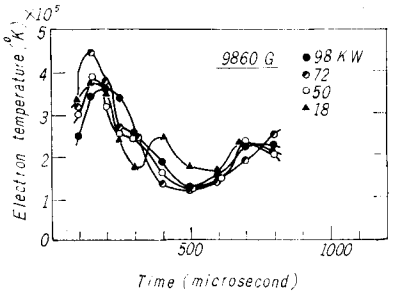

Fig. 43. Time variation of electron temperature for various powers of the *rf* generator.
Magnetic field : Heliotron type ($\lambda=1/4$), $B_0=9860$ G, $f=8.1$ Mc,
$p_0=3\times10^{-3}$ Torr $(H_2)+5\times10^{-4}$ Torr (He).

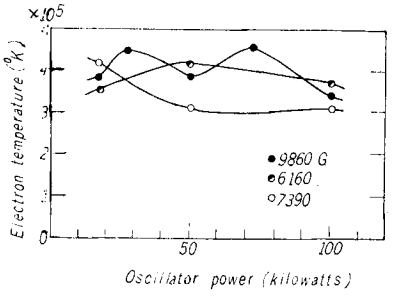

Fig. 44. Peak electron temperature as a function of the *rf* generator power for various confining fields. The condition is the same as in Fig. 43.

Ion Temperature

The confining magnetic fields used are the Heliotron field ($\lambda=1/4$) and the Bumpy torus field ($\lambda=-1/2$). The effect of the ion cyclotron heating on ion temperature is examined by changing experimental conditions as follows.

(i) To compare the ion temperature under the ion cyclotron and the Joule heatings with that under only the Joule heating.

(ii) To see the variation of ion temperature with the confining magnetic field strength.

Table 3. Ion temperature under different conditions.

$\lambda=1/4$: Heliotron type field,
$\lambda=-1/2$: Bumpy torus type field,
B_0 : Magetic field strength in the rf coil region,
V_L : One turn loop voltage for the Joule heating,
P_{rf} : Output power of the rf generator,
p_0 : Initial gas pressure of hydrogen,
T_i : Ion temperature.

λ	B_0 gauss	V_L volt	P_{rf} kilowatt	p_0 10^{-3} Torr	T_i 10^{5}°K
−1/2	2700	210	80	3.6	2.8
−1/2	4740	210	80	3.6	3.6
−1/2	4740	210	0	1.6	3.1
−1/2	4740	210	80	1.6	4.1
1/4	5500	210	0	4.0	1.2
1/4	5500	210	80	4.0	2.8

Rf frequency : 6.7 Mc

Forty times of discharge are required to take a spectrograph of spectral lines. Fig. 45 shows the microphotometric traces of the line profile of CII 4267 at the *rf* power of 73 kW and zero. In this case, the magnetic field in the *rf* coil region is set to be 1.26 times as strong as the resonant field so as to excite the ion cyclotron waves. The line width under the ion cyclotron and the Joule heatings is broader than that under only the Joule heating. Ion temperatures determined from these line widths are summarized in Table 3.

From Table 3, it becomes evident that the ion cyclotron heating can certainly raise ion temperature of plasma. The Larmar radius of C^+ becomes about 3.2 cm under the condition as the energy of C^+ is 40 eV and the magnetic field is 1000 gausses. The tube radius is 3.7 cm at the port **1.**

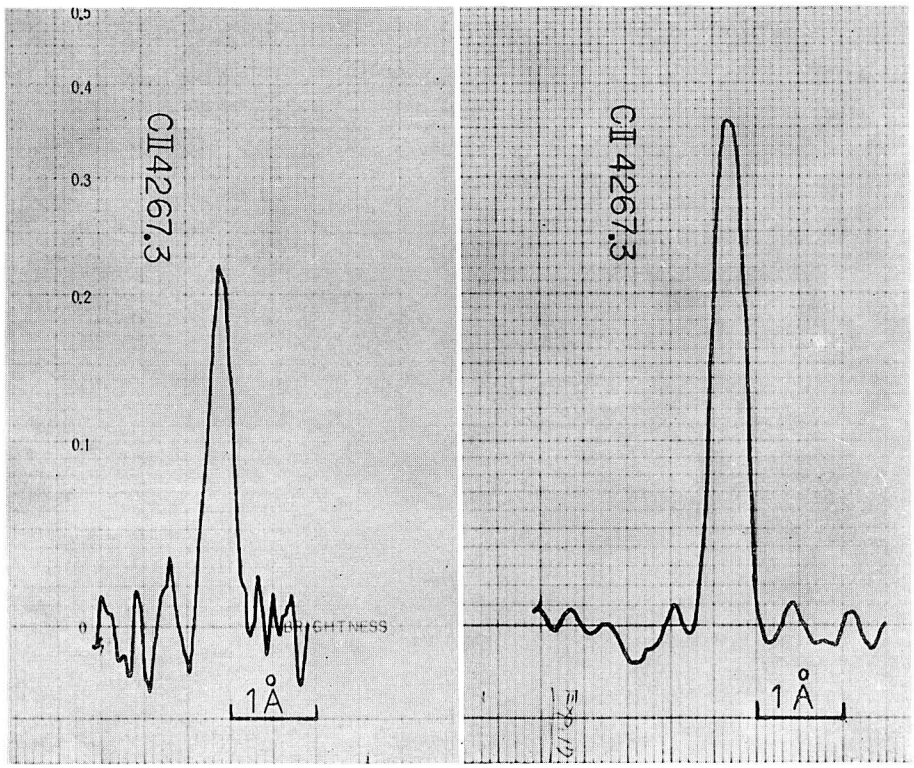

(a) (b)

Fig. 45. Microphotometer traces of the line profile of ionized carbon line CII 4267.3 for two different powers of the *rf* generator.
Magnetic field : Heliotron type ($\lambda=1/4$),
$B_0=5500$ G ($=1.26\ B_{res}$), $f=6.7$ Mc, $E_T=1.0$ V/cm,
$p_0=4\times10^{-3}$ Torr (H_2).
(a) $P_{rf}=0$
(b) $P_{rf}=73$ kW.

Therefore, ion temperature of 4×10^5 °K in Table 3 may be regarded as the upper value obtainable for C^+ under this condition. Proton temperature may be raised to higher value than 4×10^5 °K for this reason. It may also be caused for the same reason that ion temperature in the case of the Hiliotron field is somewhat lower than in the Bumpy torus field.

Information from Other Spectral Lines

Neutral helium lines and hydrogen lines of Balmar series can also be detected in the discharge of mixed gas of hydrogen and helium.

Balmar series lines (H_α, H_β, H_β, ···) decrease in intensity as the *rf* power for the ion cyclotron heating is raised up or as the confining field increases, when the Joule heating is not adopted and only the *rf* field is applied.

The half-width of H_β line is about 0.56 Å. On the other hand, the Stark broadening of the line at electron density of 10^{14} cm^{-3} is about 0.2 Å. Therefore, the Doppler broadening of the line is comparable with the Stark broadening in this case. Namely, the temperature of H is thought to be within 2×10^4 °K.

Hydrogen molecules outside N.L. surface incessantly flow into the plasma region, and they may be excited or ionized by electrons. The mean thermal velocity of hydrogen atoms at 2×10^4 °K is 1.8×10^6 cm sec^{-1}. Then their travelling time across the discharge tube is only 4.4 μ sec. Even if the hydrogen atoms are in thermal equiliblium with the tube at room temperature, the travelling time is about 36 μ sec. The life time of neutral hydrogen atoms against ionization is fairly longer than the travelling time. Therefore, most of neutral hydrogen atoms can travel through the plasma region without being subjected to ionization. In other words, the plasma can not reach a fully ionized state. This point is a defect of the Heliotron field.

6. Conclusion

Experiments on the *rf* power absorption by using a Franklin oscillator gave the information on the excitation of axisymmetric ion cyclotron waves, the occurence of ion beams and other properties of the plasma under Joule heating. Proton cyclotron waves could be excited at efficiency above 75% in hydrogen discharge. The absorption peak due to the excitation of proton cyclotron waves could be distinctly distinguished from the peak due to single-particle cyclotron resonance of protons. Ion cyclotron waves of doubly ionized helium could not be excited, owing to the little concentration of the ions.

Single-particle resonance of He^{++}, H^+ and D^+ could be detected. On the whole, their absorption peaks shifted from the associated cyclotron frequency. These shifts can be understood as Doppler shifts due to ion streams with high speed. In practice, this speed was around 10^7 cm sec^{-1} for He^{++}. This shift became small when the correction winding for the Joule heating primary current was working, so that the ion streams might be caused by the intersections of the magnetic lines of force with the stainless tube.

Experiments on the excitation and thermalization of ion cyclotron waves were carried out by using a *rf* generator of 400 kw peak power. It became evident that this ion cyclotron heating method can certainly raise the ion temperature of plasma to considerably higher temperature as 4×10^5 °K in this case, while the electron temperature is apparently insensible to the heating. If the Heliotron-B has stronger confining field, the resulting ion temperature would surely become higher.

The neutral gas flows into the plasma region under heating, that is a defect of the Heliotron-B. One countermeasure is the injection of fully ionized plasma into only the region inside the N.L. surface.

Acknowledgement

It is a pleasure for the authors to thank Dr. K. Uo and Dr. R. Itatani for their advice. Thanks are also due to Dr. R. Kato and Mr. K. Ishii for their advice and discussion of optical measurement, to Messrs H. Oshiyama, S. Ariga, M. Takahashi, and Y. Takaoka for help with experiments and to the other colleagues of the Helicon Project of Kyoto University. In addition, the help of the members of KDC-1 Computation Room in the caculations is gratefully acknowledged.

This work was supported in part by the fund of the Ministry of Education in Aid of Scientific Researches and partly by the Research Fund provided by Toyo Rayon Co..

Appendix

The electric field $\boldsymbol{E}$ induced by the current in the *rf* coil is approximately expressed in the form[16]

$$E_\theta = -E_0 I_1(\kappa r)\sin(\kappa z)\cos\omega t\,, \qquad \text{(A 1)}$$

where we have used the cylindrical coordinates and z-axis coincides with the tube axis, and I_1, κ and E_0 are the Modified Bessel function of the first kind, the axial wave number and a constant, respectively.

For simplification of analysis, we shall make the following assumptions:

(i) The oscillating component of magic field is very weak compared with the static component. Namely,

$$\left|\frac{B-B_0}{B_0}\right| \ll 1.$$

(ii) Electrical neutrality is maintained during the heating.

(iii) The variation of the transverse electric field over the Larmar radius of ions is very small.

(iv) The axial electric field vanishes due to the free motion of electrons along the magnetic field lines.

We consider a finite heating region as

$$-L \leqq z \leqq L, \qquad \text{(A 2)}$$
$$L = \frac{\pi N}{\kappa}, \quad N\text{: integer},$$

where L is the half length of the heating region.

Equation (A 1) can be rewritten in a complex notation on the above assumptions and it becomes

$$\varepsilon = (\varepsilon_+ e^{i\omega t} + \varepsilon_- e^{-i\omega t}) \sin(\kappa z). \qquad \text{(A 3)}$$

Lenard and Kulsrud[17] gave the energy dissipation rate, E.D., per unit time per unit area from the heating region, where they treated the case that the distribution function of ion velocity is the usual Maxwellian distribution. Therefore, their results are not applicable to the beam-like ions. Here we treat the case of the shifted Maxwellian distribution of ion velocity, which is expressed by

$$f(w_z) = \frac{1}{V_T\sqrt{\pi}} e^{-\frac{(w_z-u)^2}{V_T^2}}, \qquad \text{(A 4)}$$

where

$$V_T = \sqrt{\frac{2kT}{M}} \quad \text{(thermal velocity of ions)},$$

u: beam velocity,

k: Boltzmann constant,

w_z: axial velocity of ions.

Likewise to Lenard and Kulsrud's method, we get finally

$$\text{E.D.} = \frac{2n_i q^2 \varepsilon_-^2}{\sqrt{\pi}\, M\kappa^2 V_T} \int_{-\infty}^{+\infty} \frac{\sin^2\left(\pi N \frac{\zeta}{s}\right)}{|s|(1-\zeta^2)^2} e^{-(s-\delta)^2} ds, \qquad \text{(A 5)}$$

where

$$\zeta = \frac{\omega_i - \omega}{\kappa V_T}, \tag{A 6}$$

$$\delta = \frac{u}{V_T}, \tag{A 7}$$

and ω_i is the ion cyclotron frequency.

Equation (A 5) indicates the frequency dependence of the energy dissipation rate from the heating region. A term

$$\mathrm{I}(\zeta, \delta) = \int_{-\infty}^{+\infty} \frac{\sin^2\left(\pi N \frac{\zeta}{s}\right)}{|s|(1-\zeta^2)^2} e^{-(s-\delta)^2} ds \tag{A 8}$$

represents the tendency of this frequency dependence.

Computed values of $\mathrm{I}(\zeta, \delta)$ by a digital computer KDC-1 are presented in Fig. A 1 for different ζ and δ. Consequently, we can get the information as follows.

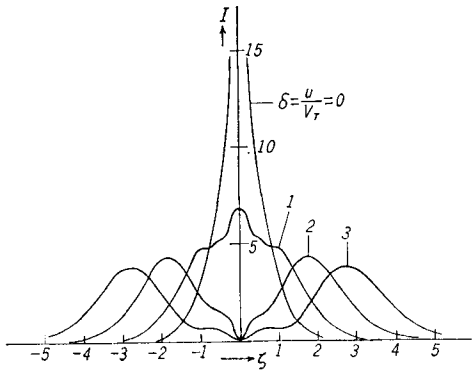

Fig. A1. $I(\zeta, \delta)$ as a function of ζ for differdet δ in the case of the Picket Fence field.

(i) For large δ, the corresponding peak of $\mathrm{I}(\zeta, \delta)$ or E.D. is situated near the position where $\zeta = \pm\delta$, i.e. $\omega = \omega_i \pm \kappa u$. In this case, the shape of the frequency spectrum of E.D. tends to resemble the simple absorption spectrum of ions with mono-energy in the axial direction. Therefore, we can determine the beam velocity from the frequency shift of the absorption curve (α curve) peak from the cyclotron frequency.

(ii) For large δ, the spectrum tends to have double peaks on both the negative and the positive sides of ζ.

(iii) The heating efficiency by single-particle cyclotron resonance rapidly decreases as δ becomes larger.

References

1) T. H. Stix; Phys. Rev., **106**, 1146 (1957).
2) T. H. Stix; J. Nucl. Energy, Part C: Plasma Phys., **2**, 84 (1961).
3) W. M. Hooke, F. H. Tenny, M. H. Brennan, H. M. Hill, Jr., and T. H. Stix; Phys. Fluids, **4**, 1131 (1961).
4) T. H. Stix; Phys. Fluids, **1**, 308 (1958).
5) A. Hasegawa and C. K. Birdsall; Phys. Fluids, **7**, 1950 (1964).
6) I. I. Bakaev, Yu. G. Zalenskii, N. L. Nazarov, A. M. Ukrainskii, and V. T. Torok; Atomnaya Energiya, **15**, 3 (1963).
7) N. M. Mather, R. G. Mills, and J. G. Murray; AEC Res. and Dev. Report, MATT-16 (1959).
8) K. Uo, A. Mohri, H. Oshiyama, R. Kato, and K. Ishii; Phys. Fluids, **5**, 1293 (1962).
9) A. Mohri, H. Oshiyama, S. Hayashi, and S. Ariga; Japan J. Appl. Phys., **2**, 815 (1963).
10) G. Gibson, W. C. Jordan, E. J. Lauer, and C. H. Woods; Phys. Fluids, **7**, 548 (1964).
11) S. P. Cunningham; AEC Report, WASH-289 (1955).
12) C. C. Lin and R. M. St. John; Phys. Rev., **128**, 1749 (1962).
13) R. J. Sovie; Phys. Fluids, **7**, 613 (1964).
14) A. Mohri and S. Hayashi; Japan. J. Appl. Phys., **2**, 306 (1963).
15) T. H. Stix and R. W. Palladino; Phys. Fluids, **3**, 641 (1960).
16) A. Mohri and S. Hayashi; Ōyo Buturi, **34**, 13 (1965).
17) A. Lenard and R. Kulsrud; AEC Report, PM-S-32, NYO-7902 (1958).